PII: S1464-1895(01)00034-5

# GNSS Occultation Sounding for Climate Monitoring

A. K. Steiner[1], G. Kirchengast[1], U. Foelsche[1], L. Kornblueh[2], E. Manzini[2] and L. Bengtsson[2]

[1]Institute for Geophysics, Astrophysics and Meteorology, University of Graz, Universitaetsplatz 5, A-8010 Graz, Austria
[2]Max-Planck-Institute for Meteorology, Bundesstraße 55, D-20146 Hamburg, Germany

**Abstract.** Considerable efforts are currently invested into the setup of a Global Climate Observing System (GCOS) for monitoring climate change over the coming decades, which is of high relevance given concerns on increasing human influences. A promising potential contribution to the GCOS is a suite of spaceborne Global Navigation Satellite System (GNSS) occultation sensors for global long-term monitoring of atmospheric change in temperature and other variables with high vertical resolution and accuracy. Besides the great importance with respect to climate change, the provision of high quality data is essential for the improvement of numerical weather prediction and for reanalysis efforts. We review the significance of GNSS radio occultation sounding in the climate observations context.

In order to investigate the climate change detection capability of GNSS occultation sensors, we are currently performing an end-to-end GNSS occultation observing system simulation experiment over the 25-year period 2001 to 2025. We report on this integrated analysis, which involves in a realistic manner all aspects from modeling the atmosphere via generating a significant set of simulated measurements to an objective statistical analysis and assessment of 2001-2025 temporal trends. © 2001 Elsevier Science Ltd. All rights reserved

## 1 Introduction

Climate change monitoring over the coming decades is of high relevance since there exists global concern that the Earth's climate is increasingly influenced by human activities (e.g., IPCC, 1995). The atmosphere plays an important role in the climate system and changes in atmospheric composition, such as increase in greenhouse gases, cause modifications of the thermal structure. High quality observations of the atmospheric state as it evolves

over time are fundamental for the analysis of atmospheric change as well as for reliable predictions of future atmospheric change.

Considerable efforts are thus currently undertaken to set up a Global Climate Observing System (GCOS), which shall enable significant advances in understanding and predicting climate variability and in detecting anthropogenic climate impacts (e.g., JSTC-GCOS, 1998). A very promising observing system in this context is a suite of spaceborne Global Navigation Satellite System (GPS and GLONASS, generically GNSS) occultation sensors for accurate global long-term monitoring of atmospheric change in temperature and other key climate variables.

The GNSS radio occultation technique is based on a satellite-to-satellite limb sounding concept using GNSS signals to probe the Earth's atmosphere. The propagation of the electromagnetic signals is influenced by the atmospheric and ionospheric refractivity field resulting in slowing and bending of the signal. The excess phase path as the principle observable is measured with millimetric accuracy. It is the basis for high quality retrievals of atmospheric key climate variables such as temperature and tropospheric water vapor. Further products include geopotential or pressure as well as ionospheric electron density.

Sensing of the terrestrial atmosphere with the radio occultation method was first practically tested with the GPS Meteorology (GPS/MET) experiment performing measurement campaigns from April 1995 to March 1997. Analysis and validation of GPS/MET data sets confirmed the particular strengths of the technique including high accuracy and vertical resolution, all-weather capability, long-term stability and global coverage (Ware et al., 1996; Kursinski et al., 1996; Rocken et al., 1997; Steiner et al., 1999; Steiner and Kirchengast, 2000; Tsuda et al., 2000).

The climate change monitoring utility of a GNSS occultation observing system has not yet been tested in any rigorous quantitative manner due to the complexity of the issue and the current lack of long-term measurements for such a study. We are currently performing a rigorous study

---

*Correspondence to*: Andrea K. Steiner

using an end-to-end GNSS occultation observing system simulation experiment over the 25-year period 2001-2025 (Kirchengast et al., 2000). The hypothesis under test is whether and to what degree a GNSS occultation observing system is able to detect climatic trends. The study is of high interest for future occultation missions and for reliable quantification of the utility of the method for GCOS.
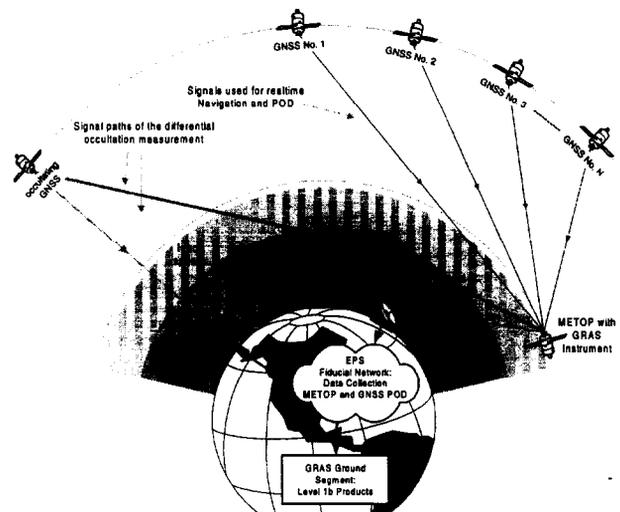
Section 2 of the paper gives a brief review of the GNSS radio occultation method and its significance in the climate observation context. In Section 3 the study design of the climate observing system simulation experiment as described by Kirchengast et al. (2000) is reviewed and we report on the current status of setting up the required tools and algorithmic components as well as on results of "testbed" simulations, which provide an indication of achievable climate monitoring performance. A summary in Section 4 concludes the paper.

## 2 The GNSS radio occultation method

The radio occultation method has its heritage in planetary radio science, where satellite-to-Earth radio links were exploited to get initial information on properties of planetary atmospheres (Fjeldbo and Eshleman, 1965; Phinney and Anderson, 1969; Fjeldbo and Eshleman, 1969; Fjeldbo et al., 1977; Lindal et al., 1990). In the case of the terrestrial atmosphere, the mean distribution of the fundamental atmospheric variables is relatively well known. Here the purpose is to measure, with global coverage, relatively small variations in order to obtain accurate data for applications such as weather prediction and climate monitoring and prediction. Since refraction effects in the terrestrial atmosphere become very small at higher altitudes (e.g., bending angle ~20 μrad only at stratopause level), high measurement accuracy is required. The successful installation of the U.S. GPS and the Russian GLONASS satellites during the last two decades, and the accurate determination of satellite positions and velocities feasible in the meantime, allow now the practical application of the radio occultation method to sense the terrestrial atmosphere (Gurvich and Krasil'nikova, 1987 (Russian original) and 1990 (English translation); Yunck et al., 1988).

### 2.1 Measurement principle

GNSS radio occultation observations are performed in an active limb sounding mode with a satellite-to-satellite geometry, which is illustrated in Fig. 1. GNSS radio signals are received by a receiver aboard a low Earth orbit (LEO) satellite. The signal path is bent and the signal retarded due to Earth's refractivity field providing phase path delay measurements (relative to propagation in vacuum). In addition, measurements of signal amplitude variations are recorded, which are caused by differential bending (leading to signal defocusing or focusing) and absorption, respectively, the latter relevant close to surface only.



Fig. 1. The radio occultation principle illustrated for the European Meteorological Operational satellite mission METOP. METOP as the LEO satellite carries the GNSS Receiver for Atmospheric Sounding (GRAS) (Source: Dornier Satellite Systems, Friedrichshafen, Germany, 1998).

### 2.2 The GPS/MET mission

The first experimental test of the GNSS radio occultation concept was the GPS/MET "proof of concept" experiment on the small LEO satellite MircoLab-1, which was led by the University Cooperation for Atmospheric Research (UCAR) (Ware et al., 1996).

The MicroLab-1 satellite was launched in April 1995, with the high performance dual frequency GPS/MET receiver aboard, into a near-circular orbit. MicroLab-1 orbited the Earth at an altitude of about 730 km with a period of about 100 min. The GPS network consists of nominally 24 satellites, each satellite continuously transmitting signals at two L-band carrier frequencies, 1575.42 MHz (L1) and 1227.60 MHz (L2). An occultation event occurs each time when the GPS satellite descends behind the Earth's limb as viewed from the aft-looking receiving antenna of the LEO satellite. With a constellation of 24 GPS satellites and one LEO satellite about 250 setting occultation events per day are possible. The GPS/MET mission provided, during its measurement campaigns from April 1995 to March 1997, approximately 100 to 150 setting occultation events per fully operational day, which is less than the possible number due to gaps in the ground tracking network and memory limitations on board of MicroLab-1 (e.g., Rocken et al., 1997; UCAR, 1998). Figure 2 shows an example of event locations for one observational day of the GPS/MET experiment (October 20, 1995). 131 occultation events were processed in this case, which are seen to be well dispersed over the entire globe.

The GPS/MET receiver collected measurements of excess phase paths (at L1 and L2 frequencies) at a sampling rate of 50 Hz. When the Anti-Spoofing encryption of the GPS signals was turned off, both L1 and L2 data were sampled at 50 Hz with equal performance, which was termed "Prime

Time" data. In the normal operational mode, the GPS signals are encrypted causing a significantly noisier L2 signal.

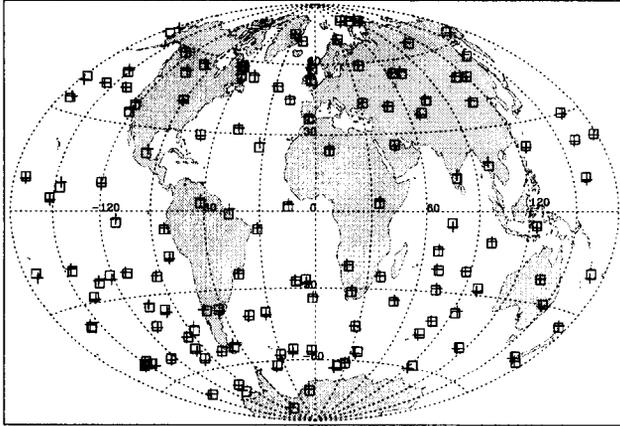GPS/MET data  Table_95.293(3)    October 20, 1995  188/131 events



**Fig. 2.** One observational day (October 20, 1995) of the GPS/MET experiment showing 131 occultation events. Each individual event is visualized by the tangent point location of a high-altitude (mesospheric) occultation ray (center of square symbol) and of the bottom-most (tropospheric) ray (plus symbol).

An occultation event lasts about 1-2 min starting at a height of about 100 km. A typical measurement profile shows phase delays of about 1 mm at the height of the mesopause (~85 km). When the signal passes through lower and denser layers of the atmosphere the delay increases via about 20 cm at stratopause level and about 20 m at tropopause level to around 1 km at the surface (~700 m in a dry atmosphere and up to ~2 km in a humid atmosphere).

An example for GPS/MET phase measurements is given in Fig. 3 showing phase paths at L1 and L2 frequencies and the ionosphere corrected LC phase, all normalized to 1 m.
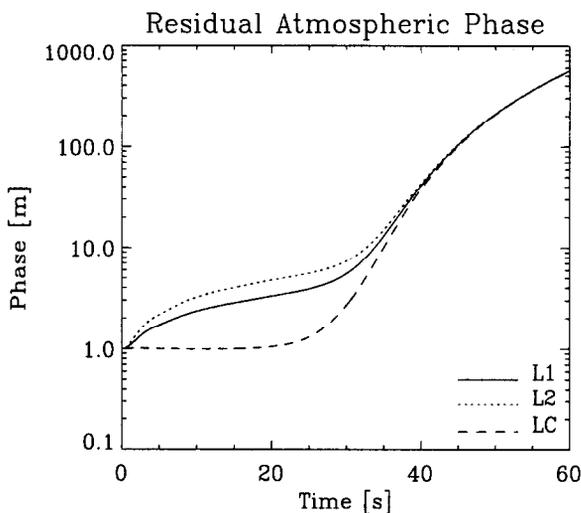
Residual Atmospheric Phase



**Fig. 3.** Measurements of residual phase delay for the L1 and L2 GPS signals as well as the ionosphere corrected path delay LC are shown. The data are from occultation event no. 7 on October 21, 1995, 03:35 UT, located at 71°S and 151.6°W.

The nominal instrumental (thermal noise limited) accuracy of the GPS/MET L1 phase measurements was 0.1 mm at 1 Hz sampling rate (Melbourne et al., 1994). The noise in LC phases, typically about 1.5 mm at 1 Hz rate, is significantly above the L1 thermal noise since several other sources contribute more to total noise (see subsection 2.4).

### 2.3 Occultation data analysis

The data analysis from phase measurements to the derivation of neutral atmospheric parameters can be divided into three steps and involves two basic principles of geometric optics. The path of a ray through a region of varying refractive index is determined globally by Fermat's principle of least time. Locally, assuming spherical symmetry, Snell's law is applied to describe the change in direction of a ray due to the refractivity field (e.g., Kursinski et al., 1997). A scheme of the data analysis is shown in Fig. 4.
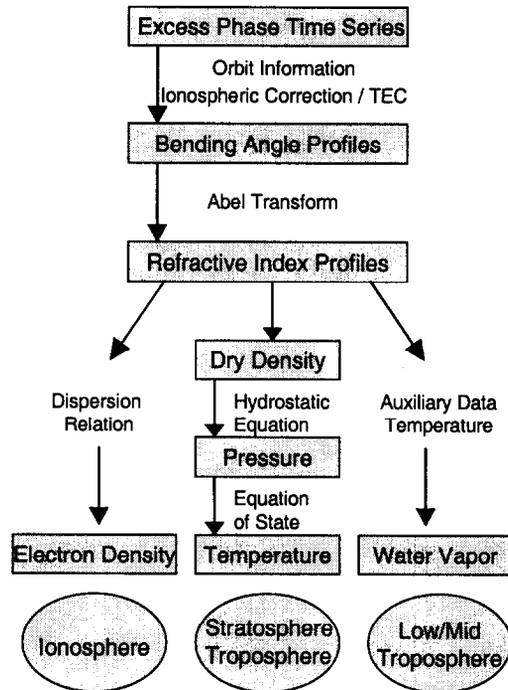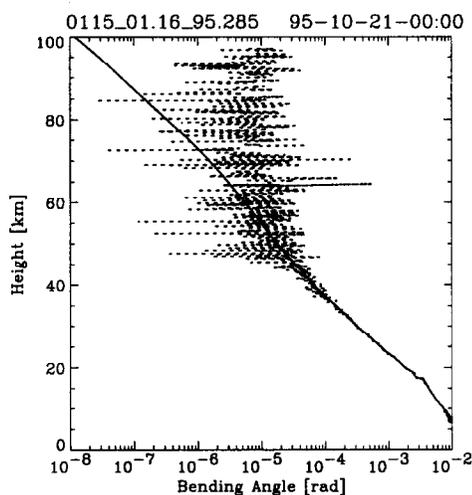


**Fig. 4.** Scheme summarizing the steps for the derivation of atmospheric and ionospheric parameters from radio occultation measurements (adapted from Høeg et al., 1995).

In the first step, the total atmospheric bending angle profile characterizing the overall effect of the atmosphere is calculated from the phase path measurements. The excess phase time series contain the ionospheric and atmospheric phase path contributions. Calculation of Doppler shifts at both frequencies and involvement of precise measurements of transmitter and receiver position and velocity gives the respective bending angle profiles as function of impact parameters. The impact parameter is defined as the perpendicular distance between the center of local curvature and the ray asymptote at the GPS or LEO. For the

derivation of neutral atmospheric parameters, the ionospheric contribution has to be removed, which can be done either by a linear combination of phases or a linear combination of bending angles, the latter giving better results (Vorob'ev and Krasil'nikova, 1994; Ladreiter and Kirchengast, 1996; Hocke et al., 1997). The residual ionospheric error is of the order of 1 cm or smaller under most ionospheric conditions but can reach several 10 cm under daytime high solar activity conditions (Ladreiter and Kirchengast, 1996).

In the second step, refractive index profiles as a function of the tangent point radius are derived from atmospheric bending angle profiles by an inversion. Given local spherical symmetry about the tangent point location, the bending angle and refractive index profiles are related via an Abel integral equation. The Abel transformation can be implemented with different inversion techniques, such as ray tracing, integral inversion, or matrix inversion methods (Hoeg et al., 1995; Kursinski et al., 1997; Hocke, 1997; Steiner et al., 1999). Above heights of about 60 km a reliable determination of bending angle data is problematic due to low signal to noise ratio. This necessitates a combination of measured bending angle data with an *a priori* or background estimate derived from climatology. An upper boundary initialization can be performed with different methods such as constant height initialization (least favorable), by use of weighting functions, or with optimal estimation methods (most favorable). The latter method gives the most probable bending angle profile and is extendable to a rigorous error analysis and characterization (Palmer et al., 2000; Healy, 2000; Rieder and Kirchengast, 2000). Figure 5 shows an example of a typical bending angle profile and its combination with model data.



Fig. 5. Bending angle profile calculated from GPS/MET phase measurement data (dotted line) for occultation event no. 115 on October 12, 1995, located at 1.1°S and 51.9°W. The profile denoted by the solid line is obtained by combination with a co-located MSISE-90 model bending angle profile (from Steiner et al., 1999).

The rms error of the GPS/MET bending angle data is typically about 1.5 μrad at 1 Hz sampling rate (Rocken et al., 1997). The combination with *a priori* data controls the errors in the measured data at high altitudes and provides a reasonable profile structure near the upper boundary for the Abelian integration.

In the third step, atmospheric parameters are calculated from the refractive index using the hydrostatic equation and the equation of state. Density, pressure, geopotential height, and temperature can be derived assuming dry air in the stratosphere and in the cold parts of the troposphere with temperatures less than about 250 K. Calculation of water vapor in the low and middle troposphere demands auxiliary temperature data.

In the lower to middle troposphere, where the fairly variable moisture distribution plays a major role, special tracking techniques in the receiver (e.g., Sokolovskiy, 2000) as well as special pre-processing of the excess phase and amplitude data are frequently necessary before the standard processing chain as described can be applied. Regarding the pre-processing, radioholographic methods including back-propagation and radio-optical processing have been shown to be of high utility (e.g., Gorbunov et al., 2000).

Furthermore, ionospheric electron density profiles can be retrieved from excess phase time series in the upper atmosphere (e.g., Leitinger et al., 1997). Also, invoking complementary ground-based total electron content (TEC) data, tomographic imaging of the ionosphere can be performed (Leitinger et al., 1997; Schreiner et al., 1999).

## 2.4. Characteristics and quality of retrieved variables

The vertical and horizontal resolution of the retrieved profiles is limited, given the usual geometric-optics model, by Fresnel diffraction and atmospheric inhomogeneities. The vertical resolution corresponds to the diameter of the first Fresnel zone, which decreases from ~1.4 km in the stratosphere to ~0.5 km near the Earth's surface. The horizontal resolution associated with this vertical resolution is about 300 km along ray and ~1.5 km across ray (e.g., Melbourne et al., 1994). Improvement of the vertical resolution is possible by applying diffraction correction based on synthetic aperture principles (e.g., Gorbunov and Gurvich, 1998).

Kursinski et al. (1997) performed an extensive error analysis on radio occultation data based on analytical methods as well as on simulations. They took into account all major error sources, including thermal receiver noise, local multipath errors, residual ionospheric errors, orbit determination errors, horizontal drift of the tangent point, initialization errors of the Abelian integral, horizontal refractivity structure and water vapor ambiguity. The error analysis was performed for different conditions.

It included a worst case scenario for daytime with solar maximum ionospheric conditions, moist atmosphere conditions, and a low signal-to-noise ratio (SNR) representing the GPS/MET receiver performance. The

retrieved temperature accuracy is better than 1 K between ~8 km and ~28 km height. Dominant error sources above 20 km are residual ionospheric error, upper boundary initialization uncertainties, and low SNR (thermal noise error), respectively. From 10 to 20 km height the horizontal refractivity structure, and below 10 km water vapor uncertainty are the limiting factors of temperature accuracy.

Alternatively, a good case scenario was performed assuming nighttime solar maximum ionospheric conditions, a dry atmosphere, and a signal-to-noise ratio representing the performance of current generation receivers (e.g., GRAS on METOP; cf. Fig. 1). The retrieved temperature accuracy was found to be less than 1 K from ~4 to ~40 km height. The dominant error sources in this case were found to be local multipath and thermal noise above ~25 km, horizontal refractivity structure from about 6 to 25 km, and water vapor uncertainty below ~6 km height.

An extensive validation of the quality of the GPS/MET neutral atmosphere soundings was done by Rocken et al. (1997). They compared GPS/MET temperature retrievals with correlative data from operational global weather analyses, radiosondes, and satellite observations. Their results reveal a 1 K mean temperature agreement with the best correlative data sets between 1 to 40 km height. Steiner et al. (1999) confirmed this data quality using a set of ~300 profiles and Steiner and Kirchengast (2000) demonstrated the utility of the data to monitor gravity waves, which has been initially proposed by Belloul and Hauchecorne (1997). Tsuda et al. (2000) confirmed that the GPS occultation technique provides important data sets for the global study of atmospheric gravity waves.

These studies established that the highest quality of the retrieved variables is achieved in the upper troposphere and lower stratosphere region with an accuracy in refractivity of better than 0.4 %, in temperature of better than 1 K, and in geopotential height of better than 20 m (Leroy, 1997). In the lower to middle troposphere, retrieval of relative humidity is possible with an accuracy of better than 10 % to 20 % (e.g., Kursinski et al., 1997).

Many GPS/MET soundings failed to penetrate the lowest 5 km of the troposphere due to signal loss by the receiver caused by atmospheric multipath effects in the presence of strong refractivity gradients. Thus current investigations regarding the performance of the GNSS radio occultation method focus on the improvement of the lower tropospheric data quality, which is of high importance for numerical weather prediction. New receivers shall be capable to reliably track signals throughout the lower troposphere down into the boundary layer. Open-loop tracking techniques are required to achieve this goal (e.g., Sokolovskiy, 2000). Algorithms for data processing in multipath areas are currently under development, a most promising route being the sensible combination of back-propagation method and radio-optical method (Gorbunov et al., 2000). Another important topic regarding retrieval improvement is the development of advanced (higher order) corrections of the ionospheric influence (e.g., Gorbunov et al., 1996; Syndergaard, 1999), which is probably the most important source of error in long-term stratospheric studies.

## 2.5 Utility for climate monitoring and other applications

The GNSS radio occultation method has great potential for climate variability and change studies since the GNSS sensors provide an unique combination of global coverage, all weather capability, high accuracy and vertical resolution, and long-term stability. The temperature accuracy is less than 1 K in the upper troposphere and lower stratosphere at a height resolution of 1-2 km. This is a key strength of the method, since indications exist that the changing thermal structure in this domain is an indicator of anthropogenic impacts due to increased greenhouse gas emissions. Of particular importance for climate studies is the long-term stability of the occultation data due to the intrinsic self-calibration. Precise clocks driven by ultrastable oscillators are the very reliable basis for highly accurate phase measurements over long times. A long-term drift of less than 0.1 K per decade should be achievable for climate monitoring purposes.

Monitoring of the predicted tropospheric warming and stratospheric cooling could be one key application of the GNSS radio occultation method. Besides temperature as an atmospheric change indicator, geopotential heights are useful to monitor the tropospheric expansion. Assimilation of occultation profiles could lead to an improvement of climate models, especially to the troposphere-stratosphere exchange dynamics modeling due to the high resolution of the occultation data at the tropopause level.

Radio occultation data have the potential to improve Numerical Weather Prediction (NWP) model analyses significantly through assimilation of bending angle or refractivity data by applying variational analysis (e.g., Palmer et al., 2000). Furthermore, the knowledge on the atmospheric momentum and energy budget could be improved through global wave activity studies with radio occultation observations (Steiner and Kirchengast, 2000; Tsuda et al., 2000). Another important application is the combination of GNSS radio occultation sensors with complementary instruments, such as stellar and solar occultation sensors or microwave limb sounders for the provision of accurate temperature and humidity retrievals from the surface up to the mesopause (Kirchengast et al., 1998; Von Engeln et al., 2000).

Monitoring of temperature, humidity, and geopotential heights should be furnished by a constellation of 5 to 25 micro-satellites carrying GNSS occultation sensors. In this respect a six satellite climate monitoring mission named Atmospheric Climate Experiment (ACE) has been proposed within the European Space Agency (ESA) Earth Explorer programme. A similar joint U.S.-Taiwan scientific project is the Constellation Observing System for Meteorology, Ionosphere and Climate (COSMIC). The COSMIC constellation is currently planned to be launched in May 2004. It also shall consist of six satellites, each with three instruments including a GPS occultation receiver, and is expected to last five years (Kuo et al., 2000; UCAR, 2000).

## 3 The GNSS climate change monitoring study

We currently undertake a large-scale climate observing system simulation study, which aims at testing the climate change detection capability of GNSS occultation sensors. A description of rationale and design and an introductory description of the main parts has been given by Kirchengast et al. (2000). The study involves five main parts of work as follows.

(i) Realistic modeling of the atmosphere (neutral atmosphere and ionosphere) over the time period 2001 to 2025.

(ii) Realistic simulations of occultation observables (excess phase path profiles) for a small GNSS receiver constellation for 2001 to 2025.

(iii) State-of-the-art data processing for temperature profile retrieval in the troposphere and stratosphere to establish a sufficient database of realistic simulated temperature measurements for 2001 to 2025.

(iv) A statistical analysis of temperature trends in both the "measured" climatology based on the database of simulated measurements and the "true" climatology from the atmosphere modeling.

(v) An assessment, by statistical inference, of how well a GNSS occultation observing system is able to detect climatic trends in the atmospheric evolution.

In the subsections below we describe and illustrate the setup of the tools and algorithms in these parts. Results of "testbed" simulations of retrieval errors and representativeness errors (due to limited spatio-temporal sampling density) are included as well.

### 3.1 Atmosphere and ionosphere modeling

Adequate global modeling of the neutral atmosphere and ionosphere is of basic importance for this study in order to obtain realistic atmospheric profiles.

For the neutral atmosphere we employ the MAECHAM model, which is an enhanced version of the ECHAM4 AGCM (Roeckner et al., 1999) with a resolution of T42L39 and the highest model level at ~0.01 hPa (~80 km) (Manzini and McFarlane, 1998). The extension up to the mesosphere captures also middle atmosphere variability, which is important for occultation simulations with realistic error characteristics. Only upward of ~0.035 hPa (~70 km) MSISE-90 climatology is used (Hedin, 1991). Figure 6 illustrates a July 15 temperature field extracted from the JJA 1997 model data utilized as "testbed" season.

Two "time slice experiments" from 2000 to 2025 are currently ongoing. One run includes transient anthropogenic forcings due to greenhouse gases, sulphate aerosol, and ozone (GAO run). The second run is a control run ignoring these forcings (CTL run). Initial and boundary conditions and prescribed fields are based on two ECHAM4 AOGCM long-term transient integrations at T42L19 resolution (Roeckner et al., 1999; Bengtsson et al., 1999). The GCM fields are stored every 6 hours over the full simulation period so that subsequent occultation simulations can capture atmospheric variability from diurnal to decadal scales.
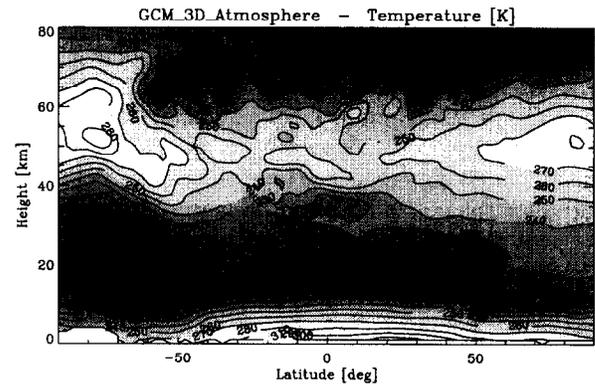


**Fig. 6.** Latitude-height plot of temperature produced by the MAECHAM T42L39 GCM for July 15, 1997, 12 UT, at 15°E.

For the ionosphere we employ the NeUoG model (Leitinger et al., 1996) which is a global empirical 3D climatology model of the ionospheric electron density field. NeUoG accounts for diurnal, seasonal, and solar-activity dependencies of the ionosphere. The suitability of the model for the present study has been confirmed by several occultation related studies (e.g., Leitinger and Kirchengast, 1997). An example for an electron density field derived with the NeUoG model is presented in Fig. 7.
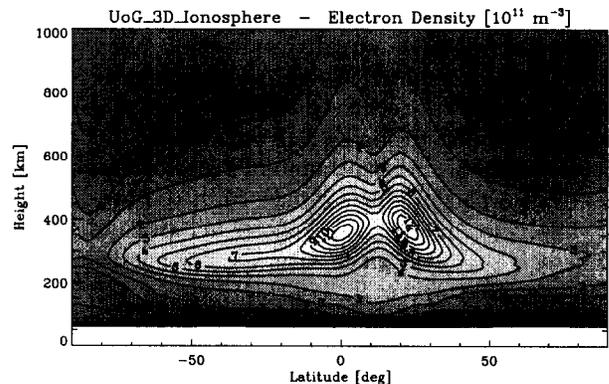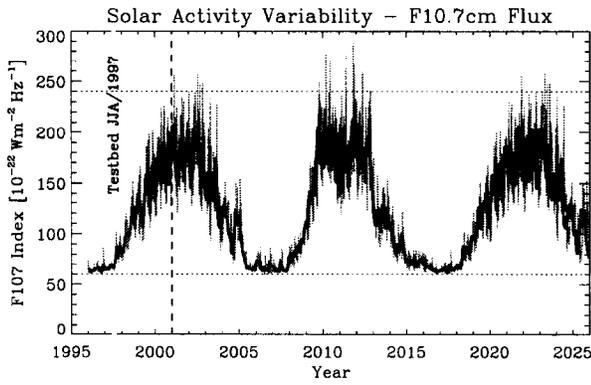


**Fig. 7.** Latitude-height plot of electron density from the NeUoG model for July, 12 UT, at 15°E.

The model is driven by day-to-day solar activity variability including the 11 year solar cycle prescribed by the F10.7 solar flux index. We use the F10.7 data set from past solar cycles 21 and 22 (1976 to 1996) as proxies for extending the current solar cycle 23 from 2001 to 2025. Weekly history averages (a good proxy for sun-induced ionospheric variations) are used as illustrated in Fig. 8. This furnishes quasi-realistic solar activity forcing of the ionosphere from diurnal to decadal scales and ensures realistic ionospheric residual errors in the retrieved atmospheric profiles, which is of importance for the error budget (Steiner et al., 1999).

Solar Activity Variability – F10.7cm Flux



**Fig. 8.** Solar activity variability with daily F10.7 flux values (gray) and monthly mean values (black). The daily values are averages over 7 days up to and including the current day ("weekly history averages").
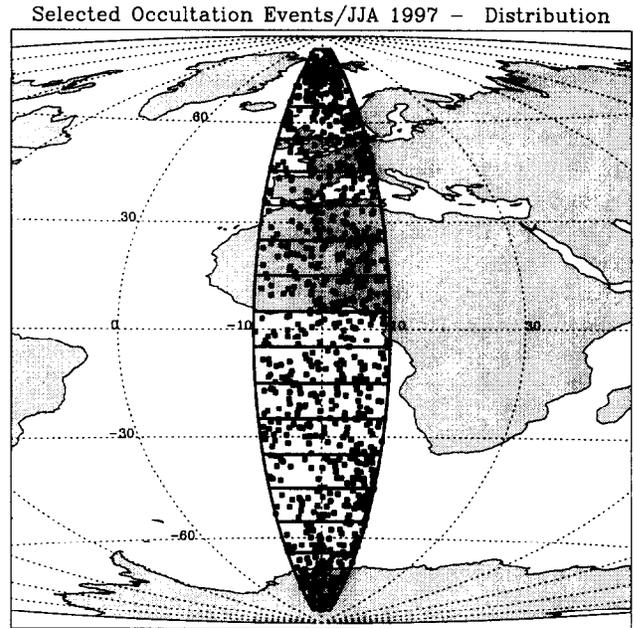
## 3.2 Simulation of occultation observations

Reflecting the typical layout of planned next generation occultation missions such as ACE and COSMIC we assumed a constellation of six LEO satellites (with an orbit selection following Kirchengast et al., 1998) equipped with GNSS receivers. Five missions, each with a lifetime of five years, cover the period from 2001 to 2025. We restricted to occultations received within an azimuthal antenna beam width of ±15° about the LEO orbit plane. These are the best qualified ones for climate purposes, since they are least sensitive to horizontal structure errors (cf. subsection 2.4) due to near-vertical tangent point trajectories in this case. The constellation yields about 2000 (rising and setting) GPS/GLONASS occultation events per day within the selected azimuthal width (nominal GNSS constellations).

In order to keep computing time at an affordable level we use a small but sensibly selected subset of these occultations only. We restrict to summer season (JJA) and to a 20° longitude sector centered over the Greenwich meridian. The latitude sector reaches from 85°N to 85°S and is divided into 17 bins with a width of 10° each. Figure 9 shows a geographic map with the selected domain.

Actual observation simulations are performed for about 1000 occultation events per season well distributed in space (see Fig. 9) and time within the selected domain, which yields about 55 to 60 events per bin. Higher event density in bins at higher latitudes is intentional as the atmospheric variability is typically higher there. For all 25 years and the two GCM runs this makes a total of ~50000 occultation events to be simulated.

For each event, the geometrical configuration is computed based on Keplerian orbit elements. Then the signal propagation through the atmosphere-ionosphere system as seen by the sensor is simulated at 10 Hz sampling rate using a sub-millimetric precision 3D ray tracer. Finally, the measured excess phase path and amplitude profiles are simulated by modifying the signal profile with the effects of the instruments and raw processing system including precise orbit determination (POD) errors, antenna gain pattern, receiver noise, local multipath, clock drifts and GNSS clock correction/single-differencing errors,
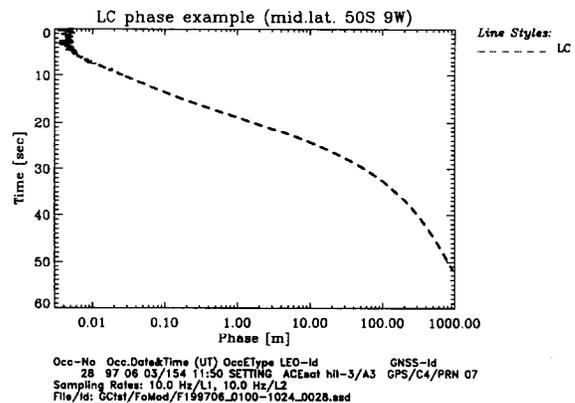
respectively. The ray tracer noise, closely white Gaussian at a magnitude of up to 1 mm, appears as part of the thermal noise of the receiver.

Selected Occultation Events/JJA 1997 – Distribution



**Fig. 9.** Selected geographic domain with a longitude range from 10°W to 10°E and a latitude range from 85°N to 85°S, divided into 17 latitude bins. Occultation events selected in JJA 1997 are indicated by black squares.

These computations are performed with a node-parallelized new version of the forward modeling part of the End-to-end GNSS Occultation Performance Simulator (EGOPS), a comprehensive tool which allows to simulate quasi-realistic occultation observables (Kirchengast, 1998). The simulation of the full observables database for ~50000 events is, besides the T42L39 GCM simulations, the computationally most time consuming part of the study.
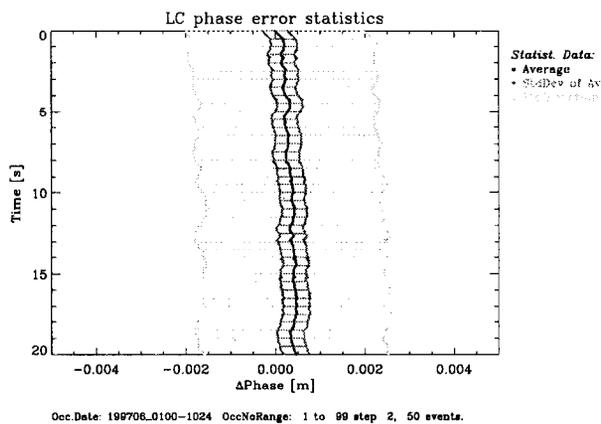
A typical example for a simulated excess phase observable is shown in Fig. 10; a quite realistic profile including ionospheric residual errors due to the realistic simulation of the ionosphere.

LC phase example (mid.lat. 50S 9W)



Occ-No   Occ.Date&Time (UT) OccEType LEO-Id        GNSS-Id
    28   97 06 03/154 11:50 SETTING ACEsat hii-3/A3 GPS/C4/PRN 07
Sampling Rates: 10.0 Hz/L1, 10.0 Hz/L2
File/Id: GCtsl/FoMod/F199706_0100-1024_0028.asd

**Fig. 10.** Typical example for simulated ionosphere-corrected excess phase path profiles.

The statistical analysis design with 17 latitude bins yields about 50 to 60 profiles per bin given about 1000 profiles per JJA sample. A validation of this design with respect to both "instrumental" bias errors in the bins (from systematic errors in retrieved temperature profiles against co-located "true" profiles) and "representativeness" errors (from spatio-temporal undersampling of variability in a bin by 50 to 60 profiles only) has been carried out for a set of simulations using MAECHAM JJA 1997 "testbed" fields.

Regarding instrumental errors we used samples of 50 events to perform a statistical error analysis. Figure 11 shows the statistical phase error of the ionosphere-corrected phase LC for a typical set of 50 occultation events (spread over the full domain shown in Fig. 9 and over 10 days). The LC phase standard deviation at 10 Hz sampling is found at a level of ~2 mm, which is in very good agreement with error levels of the new generation of GNSS receivers, in particular the METOP/GRAS performance (GRAS-SAG, 1998). This confirms that the EGOPS error simulations outlined above, where instrument parameters for GRAS were supplied without any tuning, are working in a fairly realistic way, which gives confidence in the reliability of simulated observables (e.g., Fig. 10).



**Fig. 11.** LC (ionosphere corrected) phase error statistics for 50 events showing the mean (black), the standard deviation (light gray), and the error of the mean (dark gray).
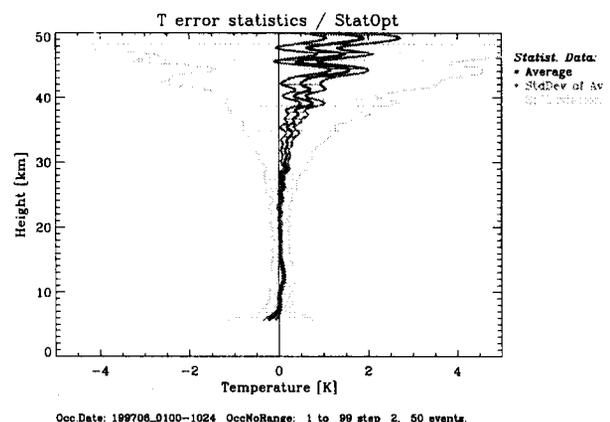
## 3.3 Temperature profiles retrieval

A database of retrieved temperature profiles is produced from the simulated observables database using a modified retrieval chain of the EGOPS tool based on the algorithmic scheme of Syndergaard (1999).

Each excess phase profile is inverted to a bending angle profile and the best-fitting (around the stratopause) MSISE-90 model bending angle profile is searched within the full lat/lon/month model domain. For the combination of the "measured" bending angle profile with the best-fitting model bending angle profile, an optimal estimation scheme is applied (Healy, 2000). The variance of the bending angle data is estimated for each individual profile at mesospheric heights (which is also used as quality indicator in that

profiles with standard deviations > 2.5 μrad are excluded from statistics, practically applying to only ~1–3 % of them). For the co-variances, a correlation length of 1 km is adopted in line with the correlation properties estimated by Syndergaard (1999). The covariance matrix for the model profiles is created adopting a reasonable uncertainty of 20 % and a correlation length of 6 km (order of a scale height) for the fairly smooth MSISE-90 bending angle profiles (cf. Hocke, 1997; Healy, 2000).
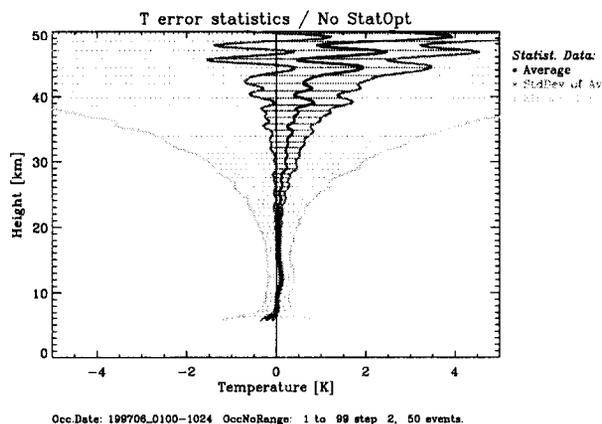
Temperature profiles are computed, assuming a dry atmosphere, based on standard formulae (Syndergaard, 1999). We use dry rather than actual temperature as our primary variable, i.e., we generally compare to "true" dry temperature profiles from the GCM model. This implies that our temperature profiles have increasingly subsumed moisture effects (and also moisture trends) below ~10 km. The dependence of dry temperature on actual temperature and humidity is accurately known (via the refractivity formula) so that we can carefully track the degree of influence of moisture.

After running the retrieval chain, utilizing the EGOPS inversion/retrieval framework, the differences between retrieved temperature profiles and the co-located "true" GCM reference profiles were computed for the set of 50 profiles prepared above. This allows inspection of the instrumental bias errors (and standard deviations) in temperature; the results are illustrated in Fig. 12. Figure 12 reveals that the biases are below 0.2 K from about 8 to 30 km, and below 0.5 K up to about 40 km. Analogous statistics with 100 events (not illustrated) show that the bias is further reduced while the standard deviation exhibits no more change, confirming the quality of the retrieval scheme. The results illustrated by Fig. 12 are very encouraging as they indicate that instrumental biases are sufficiently low for climate monitoring purposes even under realistic conditions as mimicked here.



**Fig. 12.** Temperature difference error statistics for 50 events retrieved with statistical optimization showing the mean (black), the standard deviation (light gray), and the error of the mean (dark gray).

For comparison the same temperature difference statistics were computed for temperature retrievals without statistical optimization, which one might expect to be a preferable treatment for climatological use of the data (Rocken et al., 1997). Figure 13 shows the results for the best case found (upper boundary at 60 km, heights above and below produced much worse results). The standard deviation is much larger while the bias is comparable up to about 40 km (though with larger uncertainty). However, 100 event statistics show this bias to be systematic, even slightly increased compared to 50 events, rather than to be reduced by more events in the sample. This implies that sensible optimization also helps for climate monitoring purposes.
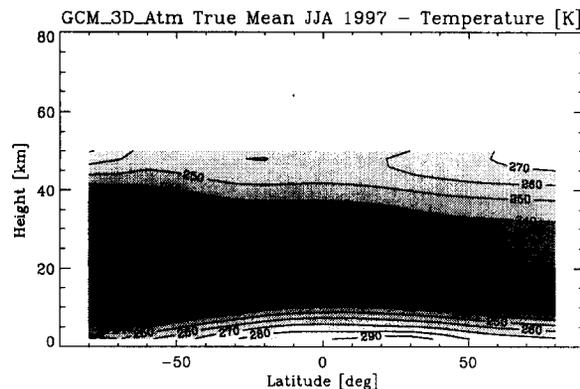


**Fig. 13.** Temperature difference error statistics for 50 events retrieved without statistical optimization showing the mean (black), the standard deviation (light gray), and the error of the mean (dark gray).

## 3.4 Temperature trend analysis

A climatological latitude-height slice dataset, termed "measured" climatology, is produced from the retrieved temperature profiles. For each of the 50 JJA samples (25 years, 2 runs) a latitude-height matrix is created with 17 latitude bins and 34 height levels (within 2 to 50 km, core region 8 to 40 km), yielding a 17 x 34 matrix. For reference, a "true" climatology matrix is computed on the same grid based directly on the GCM temperature fields in the selected space-time domain. The difference of the two matrices is a direct quantification of the total error (instrumental and representativeness) associated with each matrix element. An example of a seasonal averaged "true" GCM temperature field is presented in Fig. 14.

Furthermore, for each bin the "true" profiles from the GCM fields are computed co-located with all relevant occultation locations (about 50–60 per bin) in order to estimate the instrumental errors illustrated in Fig. 12 from retrieved-minus-true difference profiles. These error estimates are again gathered on the same grid and used for specifying the measurement errors in the trend analysis scheme. Subtracting this field from the field of total errors yields the representativeness errors.



**Fig. 14.** Example for a mean GCM temperature field in the selected latitude-height domain showing a "true" seasonal average temperature slice over the bins for the JJA 1997 "testbed" season.

We investigated the latter errors due to spatio-temporal undersampling for the JJA 1997 "testbed". The "true" climatology as defined above was computed on the 17 x 34 grid and compared to the "sampled" climatology based on mean temperature profiles per bin calculated from the GCM profiles at all selected occultation locations (about 50–60 per bin). The resulting temperature difference field is shown in Fig. 15 indicating a standard deviation of 0.51 K over the full slice and of 0.38 K within the core region from 8 to 40 km. Since maximum errors occur for southern high latitudes, considering only the northern hemisphere yields an improved standard deviation of 0.33 K. The mean difference is found to be 0.09 K only.

For reference we also made comparisons with a "sampled" climatology involving all available ~10000 occultation events; Figure 16 displays the results. In this case the standard deviation for the full slice is 0.34 K, for the core region 0.24 K, and for the northern hemisphere 0.21 K; the mean is 0.10 K. Thus a sampling density increase by a factor of 10 leads to very modest suppression of representativeness errors only, which confirms that our selection of bin and sample sizes is sensible. These results and those of further sensitivity tests (not illustrated) are again very encouraging as they indicate that representativeness errors, though they exceed instrumental biases here and there, will not obscure the climate utility of occultation measurements even when rather moderate sample sizes are used in combination with rather large bin sizes. The regions exhibiting highest representativeness error are the high latitude winter areas (see Fig. 15), well known for their large atmospheric variability.

We note that the representativeness error was computed here against T42L39 GCM fields as "true" atmosphere. Thus, a residual error due to additional variability of the real atmosphere at scales smaller than resolved by the T42L39 fields is missed to be quantified. Though this residual is expected to be small, we currently work on cross-checking the present representativeness error estimates based on fields with sufficiently high resolution (T319L60 weather analyses) in order to be confident that residual errors are practically negligible.
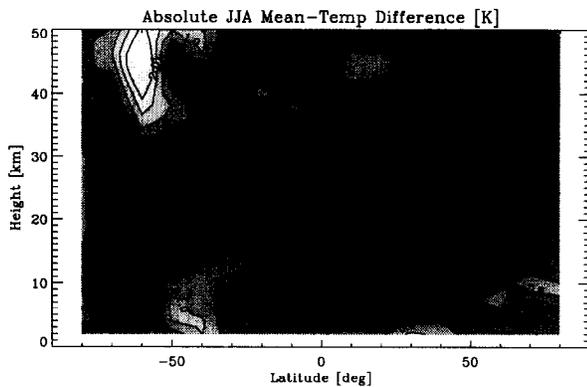
**Fig. 15.** Temperature difference between the "true" seasonal average temperature field and the "sampled" one using the selected about 50 to 60 occultation events per bin (~1000 events in total).
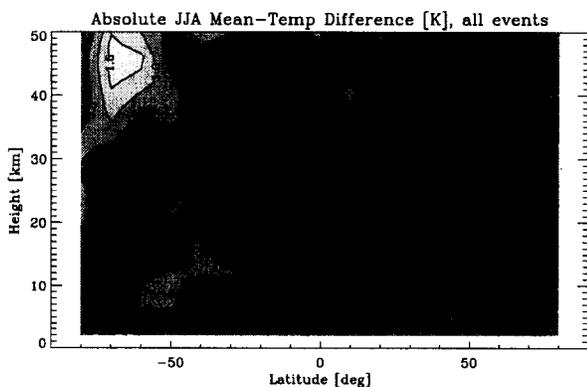


**Fig. 16.** Temperature difference between the "true" seasonal average temperature field and the "sampled" one using the total of ~10000 occultation events.

Using the prepared datasets, the trend analysis scheme is based on a multivariate weighted least-squares analysis approach and assesses the linear temporal evolution of a series of up to 25 JJA climatology matrices (up to 25 years). Its formal representation, given by Kirchengast et al. (2000), shall for the sake of brevity not be repeated here.

The scheme is used to prepare matrices of the slope of fitted trend lines and of their standard deviations. Such trend matrices (latitude-height slices) will be produced for the "measured" and the "true" climatologies for both GCM runs. Roeckner et al. (1999) included indications of the magnitude of trends to be expected over the simulated period. Given the performance indicated above, the occultation observing system should be able to reliably detect such trends within ~20 years at least in some subspaces of the outlined latitude-height slice.

### 3.5 Trend detection capability

The comparison of the trend and trend-error latitude-height slices from the "measured" climatologies of the "GAO run" and the "CTL run", respectively, is of particular interest. These data allow to assess the capability of the observing system under study for detecting presumed

anthropogenically induced trends within the time period considered. Statistical inference (hypothesis testing) will be employed for assessing trends over about 10 to 25 years, the lower bound depending on the trend results obtained. The setup for this last study part is currently under preparation.

### 4 Summary and conclusions

The GPS/MET mission was a "proof of concept" to demonstrate active limb sounding of the Earth's atmosphere using the radio occultation technique. Analysis and validation of GPS/MET data sets confirmed the key strengths of the technique including global coverage, high accuracy and vertical resolution, all-weather capability, and long-term stability, the latter property being of particular interest for climate change studies. The method can provide key atmospheric variables, most notably temperature, with high accuracy and vertical resolution in the upper troposphere and lower stratosphere domain.

Indications exist that the changing thermal structure in this domain is a particularly sensitive indicator of anthropogenic climate impacts due to increased greenhouse gas emissions. GNSS occultation sensors are expected to monitor this changing structure with a data quality surpassing any comparable observations. Temperature profile accuracy is better than 1 K at a vertical resolution of 1 to 2 km. Further climate change indicators accessible by the technique are geopotential height profiles with an accuracy of better than 20 m in the same vertical domain as temperature, and humidity profiles in the lower and middle troposphere with an accuracy of less than 10 % to 20 %.

Thus GNSS occultation observations have great potential to strongly contribute to a global climate observing system, and hence to improved climate monitoring, modeling, and prediction. Assimilation of GNSS occultation observations into numerical weather prediction models could contribute to the improvement of numerical weather analysis and prediction. Combination of GNSS occultation sensors with complementary instruments, in particular stellar and solar absorptive occultation sensors, could provide highly accurate profiles of atmospheric variables from the surface up to the mesopause.

We currently perform an ambitious GNSS climate change monitoring study, where we analyze the climate change detection capability of a GNSS occultation observing system. We focus on the atmospheric temperature change detection capability based on a realistic end-to-end observing system simulation experiment over the 25 year period from 2001 to 2025.

The study involves realistic atmosphere modeling using the MAECHAM T42L39 GCM model and realistic ionosphere modeling using the NeUoG model over the time period 2001 to 2025. Occultation observations for a small GNSS receiver constellation reflecting the typical layout of planned microsat-based occultation missions are simulated. The simulation of excess phase path profiles takes the error characteristics of the new GNSS receiver generation as well

as ionospheric residual errors realistically into account. A state-of-the-art data processing, including sensible statistical optimization, is used for temperature profile retrieval based on the phase data. "Testbed" results on instrumental bias errors and representativeness errors (due to spatio-temporal undersampling) indicate that the climate utility of the data is not diluted also under the realistic conditions of this study.

After the GCM simulations and the observables simulations are complete, temperature trends in both the "measured" climatology based on the database of simulated measurements and the "true" climatology from the GCM modeling will be computed by objective statistical analysis. Using these trend (and trend-error) results, the hypothesis under test is whether and to what degree a GNSS occultation observing system is able to detect anthropogenically induced trends in the atmospheric evolution.

The results are of immediate interest for currently prepared research and demonstration missions such as the European ACE mission and the U.S.-Taiwan COSMIC mission. They are also important to quantify to what degree a GNSS occultation observing system could become a leading backbone of the gradually implemented global climate observing system, GCOS.

For the future we consider a study expansion extending the interest to how well a GNSS occultation observing system can aid attribution of climate change.

# References

Belloul, B., and Hauchecorne, A., Effect of periodic horizontal gradients on the retrieval of atmospheric profiles from occultation measurements, *Radio Sci., 32*, 469-478, 1997.

Bengtsson, L., Roeckner, E., and Stendel, M., Why is the global warming proceeding much slower than expected? *J. Geophys. Res., 104*, 3865-3876, 1999.

Fjeldbo, G., and Eshleman, V.R., The bistatic radar-occultation method for the study of planetary atmospheres, *J. Geophys. Res., 70*, 3217-3225, 1965.

Fjeldbo, G., and Eshleman, V.R., Atmosphere of Venus as studied with the Mariner 5 dual radio-frequency occultation experiment, *Radio Sci., 4*, 879-897, 1969.

Fjeldbo, G., Sweetnam, D., Brenkle, J., Christensen, E., Farless, D., Mehta, J., Seidel, B., Michael, W., Wallio, A., and Grossi, M., Viking

radio occultation measurements of the Martian atmosphere and topography: Primary mission coverage, *J. Geophys. Res., 82*, 4317-4324, 1977.

Gorbunov, M.E., and Gurvich, A.S., Microlab-1 experiment: Multipath effects in the lower troposphere, *J. Geophys. Res., 103*, 13819-13826, 1998.

Gorbunov, M.E., Sokolovskiy, S.V., and Bengtsson, L., Space refractive tomography of the atmosphere: Modeling of direct and inverse problems, *MPIM Scient. Report No. 210*, 59 pp., MPI for Meteorology, Hamburg, Germany, 1996.

Gorbunov, M.E., Gurvich, A.S., and Kornblueh, L., Comparative analysis of radioholographic methods of processing of radio occultation data, *Radio Sci., 35*, 1025-1034, 2000.

GRAS-SAG, The GRAS instrument on Metop, *ESA/EUMETSAT Report No. VR/3021/PI (EUM No. EPS/MIS/IN/9)*, 38p., ESA/ESTEC, Noordwijk, Netherlands, 1998.

Gurvich, A.S., and Krasil'nikova, T.G., Navigation satellites for radio sensing of the Earth's atmosphere, *Sov. J. Remote Sensing, 7*, 1124-1131, 1990.

Hedin, A.E., Extension of the MSIS thermosphere model into the middle and lower atmosphere. *J. Geophys. Res., 96*, 1159-1172, 1991.

Hocke, K., Inversion of GPS meteorology data, *Ann. Geophysicae, 15*, 443-450, 1997.

Hocke, K., Kirchengast, G., and Steiner, A.K., Ionospheric correction and inversion of GNSS occultation data: Problems and solutions, *Tech. Rep. for ESA/ESTEC No.2/97*, 35 pp., Inst. of Geophys., Astrophys., and Meteorol., Univ. of Graz, Austria, 1997.

Hoeg, P., Hauchecorne, A., Kirchengast, G., Syndergaard, S., Belloul, B., Leitinger, R., and Rothleitner, W., Derivation of atmospheric properties using a radio occultation technique, *DMI Scient. Report 95-4*, 205 pp., Danish Meteorol. Institute, Copenhagen, Denmark, 1995.

Healy, S.B., Smoothing radio occultation bending angles above 40 km, *Ann. Geophys.*, revised, 2000.

IPCC, *The Science of Climate Change – Contribution of WG 1 to the 2nd assessment of the IPCC*. Cambridge Univ. Press, 572 pp, 1995.

JSTC-GCOS, Report of the 7th session of the Joint Scientific and Technical Committee for GCOS. *WMO/TD No. 857*, WMO, Geneva, Switzerland, 1998. [Available on-line from http://www.wmo.ch/web/gcos/gcoshome.html]

Kirchengast, G., End-to-end GNSS Occultation Performance Simulator (EGOPS) – Overview and exemplary applications, *Wissenschaftl. Ber. No. 2/1998*, 138 pp., Inst. for Geophys., Astrophys., and Meteorol., Univ. of Graz, Austria, 1998.

Kirchengast, G., Gorbunov, M., Jakowski, N., Kornblueh, L., Mallow, U., Rius, A., Rocken, C., Rothacher, M., Schmidtke, G., Sust, M., Ward, J., and Wernik, A., ACLISCOPE — Atmosphere and Climate Sensors Constellation Performance Explorer (ESA Earth Explorer Opportunity Mission proposal), *Wissenschaftl. Ber. No. 4/1998*, 60 pp., Inst. for Geophys., Astrophys., and Meteorol., Univ. of Graz, Austria, 1998.

Kirchengast, G., Steiner, A.K., Foelsche, U., Kornblueh, L., Manzini, E., and Bengtsson, L., Spaceborne climate change monitoring by GNSS occultation sensors, *Proc. 11th Symp. on Global Change Studies*, AMS Annual Meeting 2000, Long Beach/CA, U.S.A., 62-65, 2000.

Kuo, Y.-H., Rocken, C., Sokolovskiy, S., Kursinski, E.R., Chu, D., and Lee, L., Constellation observing system for meteorology, ionosphere, and climate–COSMIC: An overview, *Proc. 4th Symp. on Integrated Observing Systems*, AMS Annual Meeting 2000, Long Beach/CA, U.S.A., 86-92, 2000.

Kursinski, E.R., Hajj, G.A., Bertiger, W.I., Leroy, S.S., Meehan, T.K., Romans, L.J., Schofield, J.T., McCleese, D.J., Melbourne, W.G., Thornton, C.L., Yunck, T.P., Eyre, J.R., and Nagatani, R.N., Initial results of radio occultation of Earth's atmosphere using the global positioning system, *Science, 271*, 1107-1110, 1996.

Kursinski, E.R., Hajj, G.A., Schofield, J.T., Linfield, R.P., and Hardy, K.R., Observing Earth's atmosphere with radio occultation measurements using the Global Positioning System, *J. Geophys. Res., 102*, 23429-23465, 1997.

Ladreiter, H.P., and Kirchengast, G., GPS/GLONASS sensing of the neutral atmosphere: Model independent correction of ionospheric influences, *Radio Sci., 31*, 877-891, 1996.

Leitinger, R., and Kirchengast, G., Inversion of the plasma signal in GNSS occultations – simulation studies and sample results. *Acta Geod. Geophy. Hung., 32*, 379-394, 1997.

Leitinger, R., Ladreiter H.P., and Kirchengast, G., Ionosphere tomography with data from satellite reception of Global Navigation Satellite System signals and ground reception of Navy Navigation Satellite System Signals, *Radio Sci., 32*, 1657-1699, 1997.

Leitinger, R., Titheridge, J.E., Kirchengast, G., and Rothleitner, W., A "simple" global empirical model for the F layer of the ionosphere (in German; English version avail. from corresponding author). *Kleinheubacher Ber., 39*, 697-704, 1996.

Leroy, S., The measurement of geopotential heights by GPS radio occultation, *J. Geophys. Res., 102*, 6971-6986, 1997.

Lindal, G.F., Lyons, J.R., Sweetnam, D.N., Eshleman, V.R., Hinson, D.P., and Tyler, G.L., The atmosphere of Neptune: Results of radio occultation measurements with the Voyager 2 spacecraft, *Geophys. Res. Letters, 17*, 1733-1736, 1990.

Manzini, E., and McFarlane, N.A., The effect of varying the source spectrum of a gravity wave parameterization in a middle atmosphere GCM. *J. Geophys. Res., 103*, 31,523-31,539, 1998.

Melbourne, W.G., Davis, E.S., Duncan, C.B., Hajj, G.A., Hardy, K.R, Kursinski, E.R., Meehan, T.K., Young, L.E., and Yunck, T.P., The application of spaceborne GPS to atmospheric limb sounding and global change monitoring, *JPL Publication 94-18*, 147 pp., Jet Propulsion Lab, Pasadena, CA, 1994.

Palmer, I.P., Barnett, J.J., Eyre, J.R., and Healy, S.B., A non-linear optimal estimation inverse method for radio occultation measurements of temperature, humidity, and surface pressure, *J. Geophys. Res., 105*, 17513, 2000.

Phinney, R.A., and Anderson, D.L., On the radio occultation method for studying planetary atmospheres, *J. Geophys. Res., 73*, 1819-1827, 1968.

Rieder, M.R., and Kirchengast, G., Error analysis and characterization of atmospheric profiles retrieved from GNSS occultation data, *J. Geophys. Res.*, submitted, 2000.

Rocken, C., Anthes, R., Exner, M., Hunt, D., Sokolovskiy, S., Ware, R., Gorbunov, M., Schreiner, W., Feng, D., Herman, B., Kuo, Y.-H., and Zou, X., Analysis and validation of GPS/MET data in the neutral atmosphere, *J. Geophys. Res., 102*, 29849-29866, 1997.

Roeckner, E., Bengtsson, L., Feichter, J., Lelieveld, J., and Rodhe, H., Transient climate change simulations with a coupled atmosphere-ocean GCM including the tropospheric sulfur cycle. *J. Climate, 12*, 3004-3032, 1999.

Schreiner, W.S., Sokolovskiy, S.V., Rocken, C., and Hunt, D.C., Analysis and validation of GPS/MET radio occultation data in the ionosphere, *Radio Sci., 34*, 949-966, 1999.

Sokolovskiy, S.S., Tracking of radio occultation signals from low Earth orbit, *Radio Sci.*, submitted, 2000.

Steiner, A.K., Kirchengast, G., and Ladreiter, H.P., Inversion, error analysis, and validation of GPS/MET occultation data, *Ann. Geophys., 17*, 122-138, 1998.

Steiner, A.K., and Kirchengast, G., Gravity wave spectra from GPS/MET occultation observations, *J. Atmos. Ocean. Tech., 17*, 495-503, 2000.

Syndergaard, S., Retrieval analysis and methodologies in atmospheric limb sounding using the GNSS radio occultation technique. *DMI Scient. Report 99-6*, 131 pp., Danish Meteorol. Institute, Copenhagen, Denmark, 1999.

Tsuda, T., Nishida, M., Rocken, C., and Ware, R., A global morphology of gravity wave activity in the stratosphere revealed by the GPS occultation data (GPS/MET), *J. Geophys. Res., 105*, 7257-7273, 2000.

UCAR, GPS/MET Technical Overview, 1998, [Available on-line from http://www.cosmic.ucar.edu/gpsmet/index.html], cited 2000.

UCAR, COSMIC Introduction and Overview, [Available on-line from http://www.cosmic.ucar.edu], cited 2000.

Von Engeln, A., Bühler, S., Kirchengast G., and Künzi K., Temperature profile retrieval from surface to mesopause by combining GNSS radio occultation and passive microwave limb sounder data, *Geophys. Res. Lett.*, revised, 2000.

Vorob'ev, V.V., and Krasil'nikova, T.G., Estimation of the accuracy of the atmospheric refractive index recovery from Doppler shift measurements at frequencies used in the NAVSTAR system, *Phys. of Atmos. and Oceans, 29*, 602-609, 1994.

Ware, R., Exner, M., Feng, D., Gorbunov, M., Hardy, K., Herman, B., Kuo, Y., Meehan, T., Melbourne, W., Rocken, C., Schreiner, W., Sokolovskiy, S., Solheim, F., Zou, X., Anthes, R., Businger, S., and Trenberth, K., GPS Sounding of the atmosphere from Low Earth Orbit: Preliminary results, *Bull. Am. Meteorol. Soc., 77*, 19-40, 1996.

Yunck, T.P., Lindal, G.F., and Liu, C.H., The role of GPS in precise Earth observation, paper presented at the Position, Location and Navigation Symposium, Orlando, FL, Nov. 29-Dec. 2, 1988.